Published for SISSA by Springer

Received: July 27, 2018
Revised: September 24, 2018
Accepted: October 9, 2018
Published: October 15, 2018

Loop-induced neutrino non-standard interactions

Ingolf Bischer, Werner Rodejohann and Xun-Jie Xu

Max-Planck-Institut für Kernphysik, Postfach 103980, D-69029 Heidelberg, Germany

E-mail: bischer@mpi-hd.mpg.de, werner.rodejohann@mpi-hd.mpg.de, xunjie.xu@gmail.com

Abstract: Non-Standard Interactions (NSI) of neutrinos may originate from models in which new particles interact with neutrinos. In scalar extensions of the SM, the typical approach to obtain NSI requires Fierz transformations and charged Higgses, which suffer from strong constraints from collider searches or charged lepton flavor violation processes. We propose here an alternative approach to generate NSI, namely via loop processes. We show that such loop-induced NSI from secret neutrino interactions can reach sizes of $\mathcal{O}(0.1 \sim 1)$ compared to standard Fermi interaction. This approach can also give rise to neutrino-quark NSI.

Keywords: Beyond Standard Model, Neutrino Physics

ArXiv ePrint: 1807.08102

https://doi.org/10.1007/JHEP10(2018)096

Contents

JHEP10(2018)096

1 Introduction

In the era of neutrino oscillation precision measurements, the standard three-neutrino oscillation framework is being tested with increasing precision [1–3]. Hence it is important to consider any new physics that could have significant effects on neutrino oscillations. One particularly interesting possibility is provided by so-called Non-Standard Interactions (NSI) of neutrinos, which has raised rather general interest in the literature (see, e.g., refs. [4–7] for reviews on NSI). By introducing new flavor-changing neutral-current interactions $(\overline{\nu_\alpha}\gamma^\mu\nu_\beta\overline{\psi}\gamma_\mu\psi)$ of neutrinos (ν_α, ν_β) with other Standard Model fermions ψ, such NSI cause via coherent forward scattering flavor transitions in matter, disturbing the determination of the standard neutrino physics parameters. The effects of NSI in current and future long-baseline experiments (T2K, NOνA, DUNE, etc.), especially on the determination of δ_{CP}, have been extensively studied [8–14].

From the theoretical point of view, NSI of neutrinos are well motivated. Generally speaking, neutrinos have long been considered as the portal of new physics, even more so after they were found to be massive. It is reasonable to speculate that the new physics related to neutrinos also brings new interactions to neutrinos. A well-known example is the type II seesaw model [15–17]. In this model, a scalar triplet is introduced to the SM

and acquires a small vacuum exception value to generate neutrino masses.[1] Since the triplet couples both to electrons and neutrinos, NSI of neutrinos with electrons can be generated [19]. In addition to the type II seesaw model, other scalar extensions of the SM can also generate NSI in the same way, including scalar singlet models [20–23] or two-Higgs-doublet models [24, 25], etc. In all these scalar extensions, the approach of generating NSI is to integrate out a charged scalar mediator to get scalar four-fermion interactions which are then converted by a Fierz transformation to vector form (containing γ^μ). The mediator must be charged due to the Fierz transformation rules (as we will demonstrate explicitly later), which is potentially a problem of obtaining sizable NSI because charged Higgses usually face stronger collider constraints than neutral ones.

In this paper, we propose a different way to generate NSI, namely loop-induced NSI. The approach is also based on scalar extensions of the SM,[2] but without using Fierz transformations. Instead, as the name implies, the loop-induced NSI are generated by loop diagrams. Although loop contributions are in general expected to be subdominant compared with tree level contributions, in some models this way can produce fairly sizable NSI which is absent at tree level. The advantage of loop-induced NSI compared to the usual one obtained by the Fierz transformation and charged Higgses is that the source of flavor violation can be confined to the neutrino sector with "hidden" scalar interactions. Hence, large NSI can be obtained without causing problems in other well-measured processes. Other scenarios can also give rise to neutrino-quark NSI, which are absent in the previous models.

The remainder of this paper is organized as follows. In section 2, we first briefly review how NSI can be generated in scalar models by Fierz transformations, and then introduce our concept of generating NSI by loop diagrams, with some general results presented while the detailed calculation is delegated to the appendices. Then we apply the results to several explicit models in section 3.1 to 3.3. Confronting these models with experimental constraints, we estimate the order of magnitude of the loop-induced NSI in these models in section 4. Finally we conclude in section 5.

2 General analysis

In this section, we study the generation of NSI in a general framework which introduces a new scalar boson ϕ. It has Yukawa interactions with neutrinos and probably other SM fermions. Let us consider how the following NSI may be generated,

$$\mathcal{L}_{\rm NSI} = \frac{G_F}{\sqrt{2}} \epsilon^{\psi}_{\alpha\beta} \overline{\psi} \gamma^\mu \psi \overline{\nu_\alpha} \gamma_\mu P_L \nu_\beta, \tag{2.1}$$

Here $P_L \equiv (1-\gamma^5)/2$ and ψ stands for electrons or quarks which can be chiral (e.g. $\psi = e_L$, u_R, $d_L, \cdots$). Throughout the paper, we use α, $\beta, \cdots$ to denote the flavor indices.

[1] See [18] for a recent analysis on how to achieve this.

[2] Gauge extensions may also generate NSI of neutrinos, by integrating out a flavor-sensitive Z', e.g., in gauged $L_\mu - L_\tau$ models [26]. One can also imagine scenarios in which Z' models generate NSI via loops. Here we focus on the scalar case, since the scalar sector is the least experimentally tested, leaving a larger parameter space unexplored.

JHEP10(2018)096

In practice, NSI are usually expressed in terms of non-chiral neutrons (n), protons (p) and electrons (e):

$$\mathcal{L}_{\rm NSI} = \frac{G_F}{\sqrt{2}}\overline{\nu_\alpha}\gamma_\mu P_L \nu_\beta \Big[\overline{e}\gamma^\mu \left(\epsilon^{e,V}_{\alpha\beta} + \epsilon^{e,A}_{\alpha\beta}\gamma^5\right) e + \overline{n}\gamma^\mu \left(\epsilon^{n,V}_{\alpha\beta} + \epsilon^{n,A}_{\alpha\beta}\gamma^5\right) n + \overline{p}\gamma^\mu \left(\epsilon^{p,V}_{\alpha\beta} + \epsilon^{p,A}_{\alpha\beta}\gamma^5\right) p\Big]. \tag{2.2}$$

The NSI couplings in eq. (2.2) can be connected to the chiral form in (2.1) by[3]

$$\epsilon^{e,V}_{\alpha\beta} = \epsilon^{e_L}_{\alpha\beta} + \epsilon^{e_R}_{\alpha\beta}, \qquad \epsilon^{e,A}_{\alpha\beta} = \epsilon^{e_R}_{\alpha\beta} - \epsilon^{e_L}_{\alpha\beta}, \tag{2.3}$$

$$\epsilon^{n,V}_{\alpha\beta} = (\epsilon^{u_L}_{\alpha\beta} + \epsilon^{u_R}_{\alpha\beta}) + 2(\epsilon^{d_L}_{\alpha\beta} + \epsilon^{d_R}_{\alpha\beta}), \qquad \epsilon^{p,V}_{\alpha\beta} = 2(\epsilon^{u_L}_{\alpha\beta} + \epsilon^{u_R}_{\alpha\beta}) + (\epsilon^{d_L}_{\alpha\beta} + \epsilon^{d_R}_{\alpha\beta}). \tag{2.4}$$

Currently the experimental constraints on these NSI parameters, depending on the specific channels, range from $\mathcal{O}(10^{-2})$ to $\mathcal{O}(1)$ — for a recent update, see ref. [7].

To obtain the operator in eq. (2.1), we need two essentials: one is flavor-sensitive interactions of the new scalar boson and the other is the conversion of the scalar form[4] to vector form. More technically, the NSI operators contain γ^μ while the new scalar boson only introduces interactions which do not contain γ^μ. Here we introduce two approaches to achieve the conversion, by the Fierz transformation and by loop corrections. We will refer to the corresponding NSI as Fierz-transformed NSI and loop-induced NSI respectively.

2.1 Fierz-transformed NSI

Applying the Fierz transformations in some scalar extensions of the SM (e.g. the type II seesaw model) to obtain NSI has been considered in the literature [19, 21, 24, 27]. Generally, if a heavy scalar boson ϕ has Yukawa interactions $\overline{\psi_1}\psi_2\phi$ and $\overline{\psi_3}\psi_4\phi$, integrating it out will lead to the four-fermion effective operator $\overline{\psi_1}\psi_2\overline{\psi_3}\psi_4$. The Fierz transformation (see, e.g., [28]) of this operator gives

$$\begin{aligned}\overline{\psi_1}\psi_2\overline{\psi_3}\psi_4 = & -\frac{1}{4}\overline{\psi_1}\psi_4\overline{\psi_3}\psi_2 - \frac{1}{4}\overline{\psi_1}\gamma^5\psi_4\overline{\psi_3}\gamma^5\psi_2 - \frac{1}{4}\overline{\psi_1}\gamma^\mu\psi_4\overline{\psi_3}\gamma_\mu\psi_2 \\ & + \frac{1}{4}\overline{\psi_1}\gamma^\mu\gamma^5\psi_4\overline{\psi_3}\gamma_\mu\gamma^5\psi_2 - \frac{1}{8}\overline{\psi_1}\sigma^{\mu\nu}\psi_4\overline{\psi_3}\sigma_{\mu\nu}\psi_2,\end{aligned} \tag{2.5}$$

where the third term on the right-hand-side is a vector form interaction. Recall that only the vector form interaction leads to NSI effects in terrestrial matter [29]. In the SM and many extensions, the Yukawa interactions are based on chiral fermions. So it is also useful to provide the Fierz transformations of chiral fermions:

$$\overline{\psi_1}P_L\psi_2\overline{\psi_3}P_L\psi_4 = \overline{\psi_{1R}}\psi_{2L}\overline{\psi_{3R}}\psi_{4L} = -\frac{1}{2}\overline{\psi_1}P_L\psi_4\overline{\psi_3}P_L\psi_2 - \frac{1}{8}\overline{\psi_1}\sigma^{\mu\nu}P_L\psi_4\overline{\psi_3}\sigma_{\mu\nu}P_L\psi_2, \tag{2.6}$$

$$\overline{\psi_1}P_L\psi_2\overline{\psi_3}P_R\psi_4 = \overline{\psi_{1R}}\psi_{2L}\overline{\psi_{3L}}\psi_{4R} = -\frac{1}{2}\overline{\psi_1}\gamma^\mu P_R\psi_4\overline{\psi_3}\gamma_\mu P_L\psi_2, \tag{2.7}$$

[3] Axial NSI of nucleons or electrons are not important in neutrino oscillations, we hence ignore this part in this paper.

[4] In this paper, we refer to fermion interactions with the Dirac matrices $\mathbf{1}$, γ^5, γ^μ, $\gamma^\mu\gamma^5$, and $\sigma^{\mu\nu}$ between the fermion fields as scalar, pseudo-scalar, vector, axial-vector, and tensor forms, respectively. For example, $\overline{\psi}\gamma^\mu\psi A_\mu$ and $\overline{\psi}\gamma^\mu\psi\overline{\psi}\gamma^\mu\psi$ are vector form interactions; $\overline{\psi}\psi\phi$ and $\overline{\psi}\psi\overline{\psi}\psi$ are scalar form interactions.

JHEP10(2018)096

which can be obtained by replacing $(\overline{\psi_1},\ \psi_2,\ \overline{\psi_3},\ \psi_4)$ in eq. (2.5) with $(\overline{\psi_{1R}},\ \psi_{2L},\ \overline{\psi_{3R}},\ \psi_{4L})$ and $(\overline{\psi_{1R}},\ \psi_{2L},\ \overline{\psi_{3L}},\ \psi_{4R})$. It is noteworthy that eq. (2.6) produces only scalar and tensor form interactions while eq. (2.7) produces only vector form interactions. Therefore, in a chiral theory only when the effective operator has a chirality structure as in eq. (2.7), the vector form NSI can be obtained.

If eq. (2.5) or eq. (2.7) is used to generate NSI, we should identify ψ_2 and $\overline{\psi_3}$ with neutrinos, and ψ_4 and $\overline{\psi_1}$ with electrons or quarks. Note that ψ_1 and ψ_4 need to be identical to generate NSI terms from coherent forward scattering in matter. This is clear from comparing eqs. (2.5), (2.7) with eq. (2.1). In addition, limits from flavor physics strongly contrains cases with $\psi_1 \neq \psi_4$. Hence we can infer that the effective operator before the Fierz transformation should be $\overline{\psi}\nu_L\overline{\nu_L}\psi$, where ψ stands for charged fermions. Since $\overline{\psi}\nu_L$ and $\overline{\nu_L}\psi$ have nonzero electric charges, the new scalar boson must be charged. If ψ is a quark, then the scalar boson has to be colored. Such leptoquarks are severely constrained.

In conclusion, the Fierz transformation approach requires a charged scalar boson to generate NSI. If the boson is a singlet under $\mathrm{SU}(3)_c$, then neutrino-quark NSI can not be generated. Note further that since strong limits on additional charged scalars exist, the particle responsible for the Fierz-transformed NSI can not be light (MeV-scale), which is often discussed (see e.g. [30, 31]) in the context of matter-induced NSI by coherent forward scattering.

2.2 Loop-induced NSI

We will demonstrate now that if neutrinos have Yukawa interactions with a new scalar boson, then NSI can be generated at the loop level.[5] Both neutral and charged Higgses can generate such terms. Here we discuss two possible diagrams for loop-induced NSI, as shown in figure 1. The first one is based on loop corrections to the neutrino-Z vertex (left panel) which we will refer to as the triangle diagram. The other is a box diagram, which consists of pure Yukawa interactions and does not involve any gauge interactions. The external fermion lines are two neutrinos of different flavor, and two charged fermions, which can be either electrons or quarks. The internal fermion lines can be charged or neutral fermions and do not need to be identical, depending on the models. As discussed above, the two external charged fermions should be identical.

As we have mentioned, the flavor violation is introduced by the scalar-neutrino interactions and needs to be converted to vector form interactions. In the triangle diagram, this is achieved by the fact that the triangle loop generates an effective flavor-changing vertex $Z_\mu\overline{\nu_{L\alpha}}\gamma^\mu\nu_{L\beta}$. In the box diagram, the effective four-fermion operator also has γ^μ's between the fermion fields because of the internal fermion propagator.

In computing the loop-induced NSI, we need to consider the UV divergences. By simple power counting, one can see that the triangle diagram contains a logarithmic UV divergence $\int^\Lambda d^4k\frac{1}{k^4} \sim \log\Lambda$ while the box diagram is not divergent because $\int d^4k\frac{1}{k^6}$ is finite. In a renormalizable model, the UV divergence in any physical process should be

[5]Note that in the SM loop-induced and flavor-diagonal NSI are present. Their magnitude can be estimated to be of order $\epsilon \sim m_\tau^2/(16\pi^2 m_W^2) \sim 10^{-6}$, hence completely negligible.

JHEP10(2018)096

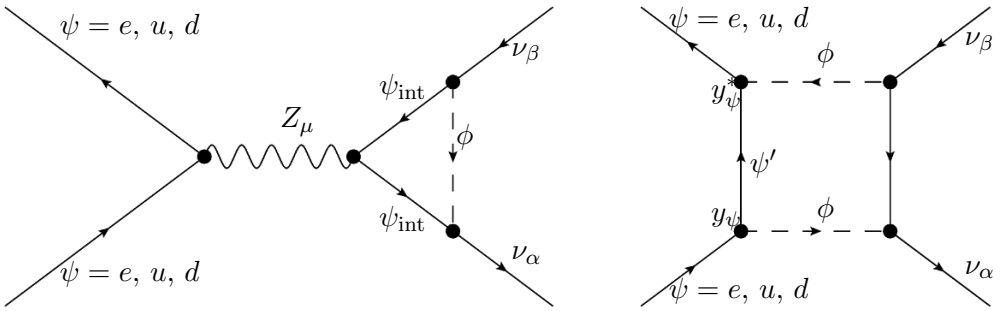

Figure 1. Triangle and box diagrams which generate the NSI in eq. (2.18).

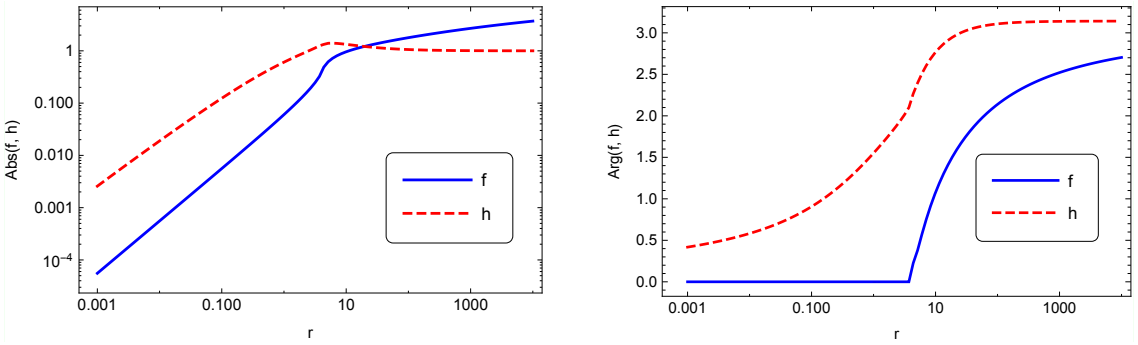

Figure 2. Numerical values of the functions $f(r)$ and $h(r)$ in eq. (2.8) with $r \equiv m_Z^2/m_\phi^2$.

canceled by adding all relevant diagrams and counterterms together. For the triangle diagram considered here, because at tree level the neutral current interactions are flavor conserving, there is no corresponding counter term. Therefore in a renormalizable and complete model, one simply needs to sum over the relevant diagrams to obtain a finite result. In one of the models considered below, the cancellation of divergences is ensured by the conservation of the gauge charges.

Triangle diagrams: in appendix A, we compute the triangle diagram and the result is presented as follows. If the UV divergences cancel out, the effective flavor changing $Z-\nu$ vertex in figure 1 is

$$\mathcal{L}_{\rm eff} = g^{(1)}_{\alpha\beta} Z_\mu \overline{\nu_\alpha} \gamma^\mu P_L \nu_\beta, \ \text{(no sum over } \alpha,\ \beta),$$

$$\text{with} \qquad g^{(1)}_{\alpha\beta} = \frac{y^*_\alpha y_\beta}{16\pi^2} \frac{g}{c_W} \frac{m_Z^2}{m_\phi^2} \left[f(r) Q_Z^{(\nu_L)} + h(r) Q_Z^{(\psi_{\rm int})} \right]. \tag{2.8}$$

Note that this result is derived under the assumption that the masses of the fermions involved are all negligibly small, which implies that in the limit $m_\phi \to 0$, eq. (2.8) does not give a valid result. The notations in eq. (2.8) are explained as follows:

- $\psi_{\rm int}$ is the internal fermion appearing in the triangle loop. The Yukawa vertices are formulated as

$$\mathcal{L} \supset y_\alpha \overline{\psi}_{\rm int} \phi \nu_{L\alpha} + y_\beta \overline{\psi}_{\rm int} \phi \nu_{L\beta} + \text{h.c.}, \tag{2.9}$$

JHEP10(2018)096

	ν_L	e_L	e_R	u_L	u_R	d_L	d_R	e	n	p
Q_Z	$\frac{1}{2}$	$-\frac{1}{2}+s_W^2$	s_W^2	$\frac{1}{2}-\frac{2}{3}s_W^2$	$-\frac{2}{3}s_W^2$	$-\frac{1}{2}+\frac{1}{3}s_W^2$	$\frac{1}{3}s_W^2$	$-\frac{1}{2}+2s_W^2$	$-\frac{1}{2}$	$\frac{1}{2}-2s_W^2$

Table 1. Z charges of Standard Model fermions.

which defines the Yukawa couplings y_α and y_β. In the triangle diagram, $\psi_{\rm int}$ can be any SM fermion that couples to the Z boson. In the loop calculation, we assume the fermion masses are all negligibly small compared to the boson masses (both ϕ and Z). This is fine as long as only leptons are coupling to the scalar, but one could also accomodate more exotic models where quarks including the top couple to scalars and neutrinos.

- g/c_W is the gauge coupling attached to the Z boson, and Q_Z is the corresponding Z charge of a fermion. Both are defined by the covariant derivative

$$D_\mu = \partial_\mu - i\frac{g}{c_W}Z_\mu Q_Z. \tag{2.10}$$

  For convenience we list the Z charges of the SM fermions in table 1.

- The scalar boson ϕ in the triangle loop has mass m_ϕ. Depending on models, it may also have a Z-charge $Q_Z^{(\phi)}$. In appendix A, we show that if the Z charges are conserved in the model, then the UV divergences cancel. In eq. (2.9), the Z charge conservation requires

$$Q_Z^{(\phi)} = Q_Z^{(\psi_{\rm int})} - Q_Z^{(\nu_L)}. \tag{2.11}$$

  Any renormalizable model satisfies eq. (2.11), as we demonstrate explicitely in In section 3.1.

- $f(r)$ and $h(r)$ are two finite functions of the mass ratio

$$r \equiv m_Z^2/m_\phi^2. \tag{2.12}$$

  The explicit forms of $f(r)$ and $h(r)$ are rather complicated and can be found in appendix A. These functions have simple limits for $r \gg 1$ and $r \ll 1$:

$$r \gg 1: \qquad f(r) \approx \frac{5}{4} - \frac{\log r}{2} + \frac{\pi}{2}i, \qquad h(r) \approx -1 - \frac{\log r}{r}, \tag{2.13}$$

$$r \ll 1: \qquad f(r) \approx \frac{r}{18}, \qquad h(r) \approx \frac{r}{18}(1 - 6\log r + 6i\pi). \tag{2.14}$$

  For general values of r, we numerically evaluate them and show the results in figure 2.

Given the effective $Z\overline{\nu}\nu$ vertex in eq. (2.8), the corresponding low-energy four-fermion interaction is

$$\mathcal{L}_{\rm NSI}^{\triangleright} = -\frac{G_F}{\sqrt{2}}\frac{8g_{\alpha\beta}^{(1)}}{g}Q_Z^{(\psi)}c_W\overline{\psi}\gamma^\mu\psi\overline{\nu_\alpha}\gamma_\mu P_L\nu_\beta, \tag{2.15}$$

where $G_F = \sqrt{2}g^2/(8m_Z^2c_W^2)$.

JHEP10(2018)096

Box diagrams: the box diagram is always finite. After computing the loop integral (see appendix B), we obtain the effective Lagrangian generated by the box NSI:

$$\mathcal{L}^{\square}_{\text{NSI}} = \frac{1}{16\pi^2}\frac{y^*_\alpha y_\beta |y_\psi|^2}{4m^2_\phi}\overline{\psi}\gamma^\mu\psi\overline{\nu_\alpha}\gamma_\mu P_L\nu_\beta. \tag{2.16}$$

Here we adopt the same definition of y_α and y_β as in eq. (2.8). Similar to the triangle diagram, the result is valid only if m_ϕ is well above the fermion masses. In addition, y_ψ is the Yukawa vertex marked in the box diagram in figure 1. The corresponding Yukawa interaction is

$$\mathcal{L} \supset y_\psi \overline{\psi'}\phi\psi + \text{h.c.}, \tag{2.17}$$

where ψ and ψ' are the external and internal fermion lines (left part of the box diagram).

To summarize, we combine the above loop-induced NSI as

$$\mathcal{L}_{\text{NSI}} = \left(\epsilon^{\triangleright}_{\alpha\beta} + \epsilon^{\square}_{\alpha\beta}\right)\frac{G_F}{\sqrt{2}}\overline{\psi}\gamma^\mu\psi\overline{\nu_\alpha}\gamma_\mu P_L\nu_\beta, \quad (\psi = e_L,\ e_R,\ u_L,\ u_R, \cdots), \tag{2.18}$$

with the individual contributions

$$\epsilon^{\triangleright}_{\alpha\beta} = -\frac{8g^{(1)}_{\alpha\beta}}{g}Q^{(\psi)}_Z c_W, \qquad \epsilon^{\square}_{\alpha\beta} = \frac{1}{16\pi^2}\frac{\sqrt{2}y^*_\alpha y_\beta |y_\psi|^2}{4m^2_\phi G_F}. \tag{2.19}$$

Here $\epsilon^{\triangleright}_{\alpha\beta}$ and $\epsilon^{\square}_{\alpha\beta}$ denote the contributions of the triangle and box diagrams respectively; $Q^{(\psi)}_Z$ is the Z charge of ψ (electrons/quarks) as listed in table 1, $g^{(1)}_{\alpha\beta}$ is given by eq. (2.8). Note that the fermions considered here are chiral. The usually considered vector NSI, cf. eqs. (2.3), (2.4) can be obtained by summing for the triangle diagram their corresponding Q_Z charges from table 1. The box diagram needs to be multiplied by 2. We stress here that since Yukawa couplings can be complex, the various ϵ can also be complex. This is in contrast to typical models in which integrating out a gauge boson generates NSI.

3 Application to Models

We will apply the above general results now to explicit models.

3.1 Model A: the minimal charged Higgs model

The first model we consider is a very simple extension of the SM by adding only a scalar singlet ϕ with hypercharge $Y_\phi = 1$ to the SM. After electroweak symmetry breaking, ϕ will eventually obtain one unit of electric charge. For this reason, we will refer to the model as the minimal charged Higgs model. The model has been studied in, e.g., refs. [20–22] (the latter two discuss tree-level NSI effects), and has also been considered as a part of larger SM extensions such as the Zee model [32].

Because the hypercharge is $Y_\phi = 1$, the only new Yukawa interaction allowed by symmetry is $\overline{L^c}i\sigma_2 L\phi$, where $L = (\nu_L,\ e_L)^T$ is a SM lepton doublet with hypercharge $Y_L = -1/2$; L^c is the charge conjugate of L so $\overline{L^c}$ has the same hypercharge as L; $i\sigma_2$ is necessary to form an $\text{SU}(2)_L$ invariant. Note that for any two Dirac spinors ψ_1 and ψ_2,

JHEP10(2018)096

the combination $\overline{\psi_1^c}\psi_2 = \overline{\psi_2^c}\psi_1$ is symmetric under the interchange of $1 \leftrightarrow 2$ (similar to the well-known fact that a Majorana mass matrix is always symmetric). On the other hand, the $\mathrm{SU}(2)_L$ product with $i\sigma_2$ is anti-symmetric. As a result, $\overline{L^c} i\sigma_2 L\phi$ vanishes if the two lepton doublets are of the same flavor: the Yukawa interactions of ϕ can be non-vanishing only when there are at least two different flavors. Adding the new Yukawa interactions to the SM, the Lagrangian of this model is

$$\mathcal{L} = \mathcal{L}_{\mathrm{SM}} + |D_\mu \phi|^2 - m_\phi^2 \phi\phi^* - V(\phi,\, H) \tag{3.1}$$

$$+ \left(\sum_{\alpha,\,\beta} y_{\alpha\beta} \overline{L_\alpha^c} i\sigma_2 L_\beta \phi + \mathrm{h.c.} \right), \tag{3.2}$$

where the Yukawa matrix $y_{\alpha\beta}$ is anti-symmetric. The SM Higgs doublet is denoted as H and $V(\phi,\, H)$ denotes all quartic terms involving ϕ and H together or ϕ only. The scalar mass m_ϕ^2 is assumed to be larger than the electroweak scale to avoid direct constraints from collider searches. For convenience of later use, we explicitly expand the new Yukawa terms:

$$\begin{aligned} \sum_{\alpha,\,\beta} y_{\alpha\beta} \overline{L_\alpha^c} i\sigma_2 L_\beta \phi = {} & 2y_{e\mu} \left(\overline{\nu_e^c} P_L \mu - \overline{\nu_\mu^c} P_L e \right) \phi + 2y_{\mu\tau} \left(\overline{\nu_\mu^c} P_L \tau - \overline{\nu_\tau^c} P_L \mu \right) \phi \\ & + 2y_{\tau e} \left(\overline{\nu_\tau^c} P_L e - \overline{\nu_e^c} P_L \tau \right) \phi + \mathrm{h.c.} \end{aligned} \tag{3.3}$$

The covariant derivative is

$$D_\mu \phi = \partial_\mu \phi - i g' B_\mu Y_\phi \phi, \tag{3.4}$$

where B_μ is the $\mathrm{U}(1)_Y$ gauge boson. After the Weinberg rotation,

$$\begin{pmatrix} W_\mu^3 \\ B_\mu \end{pmatrix} = \begin{pmatrix} c_W & s_W \\ -s_W & c_W \end{pmatrix} \begin{pmatrix} Z_\mu \\ A_\mu \end{pmatrix}, \quad (s_W,\, c_W) \equiv \frac{(g',\, g)}{\sqrt{g'^2 + g^2}}, \tag{3.5}$$

we obtain

$$D_\mu \phi = \partial_\mu \phi - i \frac{g}{c_W} Z_\mu Q_Z^{(\phi)} \phi - i g s_W A_\mu Q_A^{(\phi)} \phi, \tag{3.6}$$

with the Z- and electric charges

$$(Q_Z^{(\phi)},\, Q_A^{(\phi)}) = (-s_W^2,\, 1). \tag{3.7}$$

Here $Q_A^{(\phi)} = 1$ implies that ϕ has the same electric charge as the proton, $Q_Z^{(\phi)}$ is the Z charge of ϕ. The Z charges of the SM fermions have already been defined in eq. (2.10) and listed in table 1. It is important to notice that the Z charges in the Yukawa term (3.3) are conserved

$$Q_Z^{(\phi)} + Q_Z^{(\nu_L)} + Q_Z^{(e_L)} = 0, \tag{3.8}$$

which is crucial for the UV divergences in the relevant loops to cancel. Eq. (3.8) is not an accidental result because the model here is renormalizable and UV divergences should not appear in any physical processes.

Next, we shall discuss the neutrino NSI in this model, using the general results which have been obtained in section 2.

JHEP10(2018)096

Fierz-transformed NSI: we first integrate out ϕ, which generates the scalar form effective operator

$$\mathcal{L} \supset \frac{1}{m_\phi^2} 2y_{\beta e} \left(\overline{\nu_\beta^c} P_L e\right) 2y_{\alpha e}^* \left(\overline{e} P_R \nu_\alpha^c\right). \tag{3.9}$$

Because $y_{\alpha\beta}$ is anti-symmetric, β and α can only be μ or τ, but not e. So eq. (3.9) can not generate NSI between ν_e and e. According to eq. (2.7), with the replacement $(\overline{\psi_{1R}},\ \psi_{2L},\ \overline{\psi_{3L}},\ \psi_{4R}) \to (\overline{\nu_{\beta L}^c},\ e_L,\ \overline{e_L},\ \nu_{\alpha L}^c)$, we obtain

$$\mathcal{L} \supset \frac{4y_{\beta e} y_{\alpha e}^*}{m_\phi^2} \left[-\frac{1}{2}\overline{\nu_{\beta L}^c}\gamma^\mu \nu_{\alpha L}^c \overline{e_L}\gamma_\mu e_L\right] = \frac{4y_{\beta e} y_{\alpha e}^*}{m_\phi^2} \left[\frac{1}{2}\overline{\nu_{\alpha L}}\gamma^\mu \nu_{\beta_L} \overline{e_L}\gamma_\mu e_L\right], \tag{3.10}$$

where in the second step we have used the identity (C.10). Eq. (3.10) is the Fierz-transformed NSI in this model, which is only possible for coupling to electrons. We stress the known fact that only $\epsilon_{\mu\tau}$, $\epsilon_{\mu\mu}$ and $\epsilon_{\tau\tau}$ can be generated in this model via Fierz transformation, and that its magnitude is constrained to be rather small [21, 22], typically around $\mathcal{O}(10^{-3})$. The strongest constraints are from the variation of G_F extracted from μ and τ lifetimes, which are affected because the SM charged current interactions of μ and τ are directly modified by the charged Higgs introduced in this model — see ref. [21] for more detailed analyses. We will show next that loop-induced NSI terms can generate all flavor terms, though later it turns out that those terms are also constrained to be small. Nevertheless, the analysis illustrates the potential importance of loop effects.

Loop-induced NSI: without loss of generality, let us first focus on how $g_{\mu e}^{(1)}$ can be generated according to the results in section 2.2 and eq. (3.3). The relevant terms in eq. (3.3) are

$$2y_{\mu\tau}\overline{\nu_\mu^c} P_L \tau\phi - 2y_{\tau e}\overline{\nu_e^c} P_L \tau\phi = 2y_{\mu\tau}\overline{\tau^c} P_L \nu_\mu \phi - 2y_{\tau e}\overline{\tau^c} P_L \nu_e \phi. \tag{3.11}$$

By comparing this expression to eq. (2.9), we have the mapping

$$\nu_\alpha \to \nu_\mu,\ \nu_\beta \to \nu_e,\ \psi_{\rm int} \to \tau^c;\quad y_\alpha^* \to 2y_{\mu\tau}^*,\ y_\beta \to -2y_{\tau e}. \tag{3.12}$$

Using eq. (2.8) and assuming $\frac{m_Z^2}{m_\phi^2} \ll 1$, we obtain the effective Z-ν_e-ν_μ vertex

$$g_{\mu e}^{(1)} = -\frac{y_{\mu\tau}^* y_{\tau e}}{16\pi^2}\frac{g}{c_W}\frac{m_Z^2}{m_\phi^2}\frac{2}{3}\left[\frac{c_W^2}{3} - (1-2s_W^2)\left(\log\frac{m_Z^2}{m_\phi^2} - i\pi\right)\right]. \tag{3.13}$$

For other flavors, one can straightforward derive similar results accordingly. The general result is

$$g_{\alpha\beta}^{(1)} = \sum_{\delta=e,\mu,\tau} \frac{y_{\alpha\delta}^* y_{\beta\delta}}{16\pi^2}\frac{g}{c_W}\frac{m_Z^2}{m_\phi^2}\frac{2}{3}\left[\frac{c_W^2}{3} - (1-2s_W^2)\left(\log\frac{m_Z^2}{m_\phi^2} - i\pi\right)\right]. \tag{3.14}$$

Eq. (3.14) combined with eq. (2.19) gives the triangle NSI in this model:

$$\epsilon_{\alpha\beta}^{\triangleright} = -\frac{8c_W}{g}Q_Z^{(\psi)} \sum_\delta \frac{y_{\alpha\delta}^* y_{\beta\delta}}{16\pi^2}\frac{g}{c_W}\frac{m_Z^2}{m_\phi^2}\frac{2}{3}\left[\frac{c_W^2}{3} - (1-2s_W^2)\left(\log\frac{m_Z^2}{m_\phi^2} - i\pi\right)\right]. \tag{3.15}$$

JHEP10(2018)096

The box NSI in this model also exists, but only for electron-neutrino NSI because ψ in the right panel of figure 1 can only be an electron. The box NSI parameter $\epsilon^{\square}_{\alpha\beta}$ can be directly obtained from eq. (2.19) with the Yukawa couplings replaced by

$$y^*_\alpha y_\beta \to \sum_{\delta=e,\mu,\tau} 4y^*_{\alpha\delta} y_{\beta\delta}, \quad |y_\psi|^2 \to 4\left(|y_{e\mu}|^2 + |y_{e\tau}|^2\right), \tag{3.16}$$

which leads to

$$\epsilon^{\square}_{\alpha\beta} = \frac{1}{16\pi^2} \frac{4\sqrt{2}\sum_\delta y^*_{\alpha\delta} y_{\beta\delta}}{m^2_\phi G_F} \left(|y_{e\mu}|^2 + |y_{e\tau}|^2\right). \tag{3.17}$$

Recall that the usually considered vector form for ϵ is twice the value of eq. (3.17). It is noteworthy that all flavor terms $\epsilon_{\alpha\beta}$ can be generated, while the Fierz-transformed NSI was only possible for the $\mu\tau$ case.

3.2 Model B: secret neutrino interactions

Secret neutrino interactions are a type of interactions that only exist among neutrinos. They are generally difficult to be tested in terrestrial experiments because electrons and quarks are not involved in such interactions. However, secret neutrino interactions could have interesting cosmological and astrophysical effects, in supernova dynamics, cosmic neutrino propagation, Big Bang Nucleosynthesis (BBN), etc. Therefore it has been considered in many references [33–38]. The simplest secret neutrino interaction is a scalar boson interacting with the left-handed neutrinos $\phi\nu_L\nu_L$ where ν_L is in the Weyl spinor notation.[6] In the Dirac notation, and including the flavor indices, the interaction should be formulated as

$$\mathcal{L} \supset y_{\alpha\beta}\phi\overline{\nu^c_{\alpha L}}\nu_{\beta L} + \text{h.c.} \tag{3.18}$$

We demonstrate now that the secret neutrino interaction in eq. (3.18) leads to loop-induced NSI. No NSI are generated when the scalar is integrated out. Because ϕ does not couple to charged fermions in this model, the Fierz-transformed NSI and the loop-induced NSI from the box diagram are absent. Only the triangle diagram can generate NSI.

By comparing eq. (3.18) to eq. (2.9), we can use the mapping

$$y^*_\alpha y_\beta \to \sum_\delta y^*_{\delta\alpha} y_{\delta\beta}, \ \psi_{\text{int}} \to \nu^c_{\alpha L}, \ Q_Z^{(\psi_{\text{int}})} \to -Q_Z^{(\nu_L)}, \tag{3.19}$$

to find [cf. eq. (2.8)]:

$$g^{(1)}_{\alpha\beta} = \frac{1}{16\pi^2}\frac{g}{c_W} Q_Z^{(\nu_L)} \frac{m^2_Z}{m^2_\phi} \sum_\delta y^*_{\delta\alpha} y_{\delta\beta} \left[f(r) - h(r)\right].$$

Then the corresponding triangle NSI parameter in eq. (2.19) is:

$$\epsilon^{\triangleright}_{\alpha\beta} = -\frac{4}{16\pi^2} Q_Z^{(\psi)} \frac{m^2_Z}{m^2_\phi} \sum_\delta y^*_{\delta\alpha} y_{\delta\beta} \left[f(r) - h(r)\right]. \tag{3.20}$$

[6] The secret scalar boson could also couple right-handed and left-handed neutrinos together ($\phi\nu_R\nu_L$), which has different phenomenological consequences in cosmological and astrophysical processes. In this case, due to the absence of Z coupling to ν_R, there is no loop-induced NSI.

JHEP10(2018)096

Note that the internal fermions in the triangle diagram are left-handed neutrinos, and recall that $r = m_Z^2/m_\phi^2$. However, one should note that eq. (3.18) is not a complete model so the UV divergences cannot be fully canceled without introducing new particles or new interaction terms. Consequently there is a UV divergence, explicitly shown in eq. (A.14) and not given here. In a complete and renormalizable model containing the secret neutrino interaction (3.18), this UV divergence will be canceled by additional diagrams, potentially modifying the result (3.20). Since this depends on the details of the complete model, we refrain from going further into detail and keep eq. (3.20), which should be order-of-magnitude wise correct. Regarding eq. (3.18) there is not necessarily lepton number violation because ϕ could carry two units of lepton number. However, if the lepton number is violated by, e.g., non-zero $\langle\phi\rangle$, then such a secret interaction can also be responsible for a Majorana neutrino mass. If this term is the only term responsible for neutrino mass, it is interesting to note that $\epsilon^{\triangleright}_{\alpha\beta} \propto (m_\nu m_\nu^\dagger)_{\alpha\beta}$, which would result in $\epsilon^{\triangleright}_{e\mu} \simeq \epsilon^{\triangleright}_{e\tau} \ll \epsilon^{\triangleright}_{\mu\tau}$, where the proportionality factor between $\epsilon^{\triangleright}_{e\mu}$ and $\epsilon^{\triangleright}_{\mu\tau}$ is about $\Delta m^2_{21}/|\Delta m^2_{31}|$ [39].

It should be noticed that in the UV complete models containing the secret neutrino interactions, ϕ may or may not be accompanied with a charged Higgs, depending on whether ϕ is the neutral component of an $\mathrm{SU}(2)_L$ multiplet or not. The former case usually suffers from stringent constraints due to its connection with the charged Higgs — see, e.g., [25]. In the latter case, the secret neutrino interactions are usually obtained by mass mixing of left-handed neutrinos with other singlet fermions such as the right-handed neutrinos, which happens in the Majoron model [40] and its variants [41]. For such models, one needs to check whether the sizable mixing would lead to correct light neutrino masses or not. Since all these details are very model-dependent, we would refrain here from further discussions on the UV complete models of secret neutrino interactions.

Due to a lack of very stringent terrestrial constraints on the secret neutrino interactions, the loop-induced NSI in this model can be in principle much larger than in the previous model. We will discuss possible sizes of the NSI later in section 4.

3.3 Model C: neutral scalar boson

Neutrinos could also have new scalar interactions with the charged fermions mediated by a neutral scalar, which can be expressed by the following Lagrangian:

$$\mathcal{L} \supset y^\nu_{\alpha\beta}\phi\overline{\nu_\alpha}\nu_\beta + y^\psi\phi\overline{\psi}\psi + \text{h.c.} \quad (\psi = e,\ u,\ d). \tag{3.21}$$

Since neutrino-electron and coherent elastic neutrino-nucleus scattering are induced, eq. (3.21) has interesting phenomenological impact on experiments such as COHERENT [42], CONUS [43], CHARM II [44, 45], LSND [46], TEXONO [47], GEMMA [48, 49], etc., see e.g. refs. [50–52].

In this model, because the scalar boson is neutral, there is no Fierz-transformed NSI. In the triangle diagram (figure 1), since the external neutrino lines are left-handed neutrinos, the internal fermion lines can only be right-handed neutrinos[7] because $\phi\overline{\nu_\alpha}\nu_\beta = \phi\overline{\nu_{\alpha R}}\nu_{\beta L} +$

[7] One may also consider another type of ϕ-ν interaction similar to eq. (3.18). In this case, the loop-induced NSI is a combination of model B and model C — it has the same $\epsilon^{\triangleright}_{\alpha\beta}$ as model B and the same $\epsilon^{\square}_{\alpha\beta}$ as model C.

JHEP10(2018)096

	ϵ_e^F	$\epsilon_e^{\triangleright}$	$\epsilon_n^{\triangleright}$	$\epsilon_p^{\triangleright}$	$\epsilon_e^{\square}$	$\epsilon_n^{\square}$	$\epsilon_p^{\square}$
model A	$\mathcal{O}(10^{-3})$	$\mathcal{O}(10^{-5})$	$\mathcal{O}(10^{-4})$	$\mathcal{O}(10^{-5})$	$\mathcal{O}(10^{-3})$	0	0
model B	0	$\mathcal{O}(10^{-1})$	$\mathcal{O}(1)$	$\mathcal{O}(10^{-1})$	0	0	0
model C	0	0	0	0	$\mathcal{O}(10^{-2})$	$\mathcal{O}(10^{-2})$	$\mathcal{O}(10^{-2})$

Table 2. Reachable magnitude of the Fierz and loop-induced NSI in the three models under study. Here ϵ^F, $\epsilon^{\triangleright}$ and $\epsilon^{\square}$ are generated by Fierz transformations, triangle and box diagrams respectively.

$\phi\overline{\nu_{\alpha L}}\nu_{\beta R}$. Since right-handed neutrinos do not couple to the Z boson there is no triangle NSI in this model, i.e.

$$\epsilon^{\triangleright}_{\alpha\beta} = 0. \tag{3.22}$$

However, since left- and right-handed elecrons and quarks do exist, this model leads to triangle diagrams correcting their couplings to the Z boson. Therefore, the model is constrained by the partial decay widths of Z. We will discuss this issue in section 4.

On the other hand, this model has loop-induced NSI from the box diagram. By comparing eq. (3.21) to eq. (2.9) and (2.17), we have the mapping

$$y^*_\alpha y_\beta \to \sum_{\delta=e,\mu,\tau} y^\nu_{\alpha\delta} y^\nu_{\delta\beta}, \quad |y_\psi|^2 \to |y^\psi|^2, \tag{3.23}$$

which gives the box NSI parameter:

$$\epsilon^{\square}_{\alpha\beta} = \frac{1}{16\pi^2}\frac{\sqrt{2}|y^\psi|^2}{4m_\phi^2 G_F}\sum_{\delta=e,\mu,\tau} y^\nu_{\alpha\delta} y^\nu_{\delta\beta}. \tag{3.24}$$

Although eq. (3.21) is not a complete model, in contrast to model B, there is no UV divergence in computing the loop-induced NSI because the box diagram is always finite.

4 How large can loop-induced NSI be?

Now that we have derived loop-induced NSI both in the general framework and in several specific models, a natural question to ask is how large they can be. The answer of course depends on the models as well as the experimental constraints. In this section, we summarize some experimental constraints on the three models and estimate the allowed magnitude of loop-induced vector NSI for couplings to electrons, protons and neutrons, whose definition is given in eqs. (2.3), (2.4). We selectively consider three most relevant experimental constraints, namely the invisible Z decay width, elastic neutrino scattering and charged lepton flavor violation. When all these constraints are taken into consideration, we find that loop-induced NSI in the three models can reach the magnitude listed in table 2.

Invisible Z decay width: since in the triangle diagram the $Z\overline{\nu}\nu$ vertices are modified in models A and B, it is necessary to consider the effect on the invisible Z decay width which has been measured precisely [53]:

$$\Gamma_{Z,\text{inv}} = N_\nu \Gamma_{Z\to\nu\overline{\nu}}, \quad N_\nu = 2.9840 \pm 0.0082. \tag{4.1}$$

JHEP10(2018)096

Adding eq. (2.8) to the SM $Z\bar{\nu}\nu$ terms, we have the following $Z\bar{\nu}\nu$ interactions

$$\mathcal{L}_{Z\bar{\nu}\nu} = \frac{gQ_Z^{(\nu_L)}}{c_W} Z_\mu \lambda_{\alpha\beta} \overline{\nu_\alpha} \gamma^\mu P_L \nu_\beta, \text{ with } \lambda_{\alpha\beta} = \frac{g^{(1)}_{\alpha\beta}}{g} \frac{c_W}{Q_Z^{(\nu_L)}} + \delta_{\alpha\beta}. \tag{4.2}$$

For one generation of neutrinos, the decay width $\Gamma_{Z\to\nu\bar{\nu}}$ is proportional to the absolute square of the vertex coupling. Generalizing to three generations, it holds that $\Gamma_{Z,\text{inv}} \propto \text{tr}[\lambda\lambda^\dagger]$, from which we can infer

$$N_\nu = \text{tr}[\lambda\lambda^\dagger] = \sum_{\alpha,\beta} |\lambda_{\alpha\beta}|^2. \tag{4.3}$$

Therefore, the invisible Z decay width should give a strong constraint on $\text{tr}[\lambda\lambda^\dagger]$. However, one should note that even when $\text{tr}[\lambda\lambda^\dagger]$ is fixed at 3, large values of $g^{(1)}_{\alpha\beta}$ are still allowed due to cancellations in the matrix product. The constraint from invisible Z decay is only useful when it is combined with the elastic neutrino scattering constraints to be introduced next.

Elastic neutrino scattering. New neutrino interactions can be directly constrained by elastic neutrino scattering experiments [50–52, 54]. Some neutrino-electron scattering experiments (e.g. CHARM II [44, 45], LSND [46], TEXONO [47]) already have precision measurement of the SM process and most recently coherent elastic neutrino-nucleus scattering has been successfully observed and will also be precisely measured in the near future [42, 43].

In general when there are new neutrino interactions, elastic neutrino scattering is sensitive to the ratio between the new and SM cross sections (ignoring spectral effects):

$$R_\alpha \equiv \frac{\sigma_{\text{new}}(\nu_\alpha + \psi \to \nu + \psi)}{\sigma_{\text{SM}}(\nu_\alpha + \psi \to \nu_\alpha + \psi)}, \tag{4.4}$$

where the final neutrino state in the numerator can be of any flavor and the cross section σ_{new} is a sum over all possible flavors. The target particle ψ can be either an electron or a nucleus.

Considering the specific models in this paper, the $Z\bar{\nu}\nu$ vertices are modified in model A and model B, while in model A and model C the scalar bosons make tree-level contributions to neutrino-electron/nucleus scattering.

Given the modified $Z\bar{\nu}\nu$ vertices in eq. (4.2), it is straightforward to derive[8]

$$R_\alpha = \sum_\beta |\lambda_{\alpha\beta}|^2. \tag{4.5}$$

It is interesting to note that eq. (4.3) can be expressed in terms of the ratios R_α:

$$N_\nu = \text{tr}[\lambda\lambda^\dagger] = R_e + R_\mu + R_\tau. \tag{4.6}$$

[8]For $\nu_e + e$ scattering, there are also $W^\pm$ (charged current) contributions, which can be taken into account by replacing $Q_Z^{(\nu_L)}$ in eq. (4.2) with an effective value. For simplicity, in this paper we do not consider this part of contributions in our estimation of experimental constraints.

JHEP10(2018)096

According to the ν_μ and ν_e elastic scattering data [44, 46, 47], R_e and R_μ cannot have large deviations from 1:

$$\delta R_e \equiv |R_e - 1| \lesssim 20\%, \quad \delta R_\mu \equiv |R_\mu - 1| \lesssim 3\%. \tag{4.7}$$

This combined with the Z decay observation $|N_\nu - 3| \ll 1$ implies that R_τ should also be close to 1:

$$\delta R_\tau \equiv |R_\tau - 1| \lesssim 20\%. \tag{4.8}$$

Using eq. (4.2), we can convert[9] the constraints on R_α to constraints on $g^{(1)}_{\alpha\beta}$:

$$\left| \frac{g^{(1)}_{\alpha\beta}}{g} \frac{c_W}{Q_Z^{(\nu_L)}} \right| < \delta_{\alpha\beta} + \sqrt{1 + \delta R_\alpha}. \tag{4.9}$$

Thus, using eq. (2.19), the corresponding constraints on $\epsilon^{\triangleright}_{\alpha\beta}$ are

$$|\epsilon^{\triangleright}_{\alpha\beta}| < 4(\delta_{\alpha\beta} + \sqrt{1 + \delta R_\alpha})|Q_Z^{(\psi)}| = \begin{cases} \mathcal{O}(0.1) & (\psi = e \text{ or } p) \\ \mathcal{O}(1) & (\psi = n) \end{cases}, \tag{4.10}$$

where for $\psi = e$ or p the result is suppressed by their small Z charges $|Q_Z^{(e)}| = |Q_Z^{(p)}| \propto 1 - 4s_W^2$. To obtain the $\mathcal{O}(1)$ NSI in model B referred to in table 2, we can take, for example, $m_\phi = 100$ MeV and $y = 10^{-2}$, which according to eq. (3.20) should lead to $\epsilon^{\triangleright}_{\alpha\beta} = \mathcal{O}(1)$. Model A, as we discuss below, cannot induce such large NSI due to further constraints from charged lepton flavor violation.

The tree-level contribution of the scalar boson in model C is roughly

$$\delta R_\alpha \simeq \sum_\beta \left(\frac{y^\nu_{\alpha\beta} y^\psi}{m_\phi^2} \right)^2 \Big/ \left(\frac{g^2}{m_Z^2 c_W^2} \right)^2. \tag{4.11}$$

Assuming $y^\nu_{\alpha\beta} y^\psi$ is $\mathcal{O}(1)$, the box NSI in model C could reach

$$\epsilon^{\square}_{\alpha\beta} \simeq \frac{1}{8\pi^2} \sqrt{3\delta R_\alpha} \simeq \begin{cases} 1.0 \times 10^{-2} & (\text{if } \delta R_\alpha = 20\%) \\ 3.8 \times 10^{-3} & (\text{if } \delta R_\alpha = 3\%) \end{cases}. \tag{4.12}$$

We mentioned before that model C is also constrained by the partial decay widths of Z to e, u, and d. Here we can check that the constraint in eq. (4.12) is consistent with current uncertainties of the partial decay widths. Still assuming Yukawa couplings to be one, with eq. (3.24), we obtain

$$\frac{3\sqrt{2}}{8 m_\phi^2 G_F} = 3 \frac{c_W^2}{g^2} \frac{m_Z^2}{m_\phi^2} \simeq \sqrt{3\delta R_\alpha}. \tag{4.13}$$

This implies

$$\frac{m_Z^2}{m_\phi^2} \simeq 0.14\,, \quad m_\phi^2 \simeq 5.9 \times 10^4 \text{ GeV}, \tag{4.14}$$

[9] More explicitly, we first substitute the expression of $\lambda_{\alpha\beta}$ in eq. (4.2) into eq. (4.5) and then check the maximally allowed value of each $|\lambda_{\alpha\beta} - \delta_{\alpha\beta}|$ individually with R_α varying in $[1 - \delta R_\alpha,\ 1 + \delta R_\alpha]$.

JHEP10(2018)096

which can be used to study the corrected Z couplings of $\psi = e, u, d$ from triangle diagrams. We slightly modify eq. (2.8) to describe the correction to the left-handed coupling $Q_Z^{\psi_L}$ to Z by

$$\mathcal{L}_{\text{eff}} = g^{(1)}_{\psi_L} Z_\mu \overline{\psi} \gamma^\mu P_L \psi, \quad \text{with} \quad g^{(1)}_{\psi_L} = \frac{y^*_\psi y_\psi}{16\pi^2} \frac{g^3}{3c_W^3} \sqrt{3\delta R_\alpha} \left[f(r) Q_Z^{(\psi_L)} + h(r) Q_Z^{(\psi_R)} \right], \quad (4.15)$$

and likewise for the right-handed coupling. Estimating orders of magnitude,

$$1/48\pi^2 \approx 3 \times 10^{-3}, \quad g/c_W \approx 1, \quad \sqrt{3\delta R_\alpha} \approx 10^{-1}, \quad |f(r)| \approx 8 \times 10^{-3}, \quad |h(r)| \approx 0.2, \quad (4.16)$$

we get an order 10^{-5} correction to the coupling in the case of the $h(r)$ term. We conclude that the SM couplings to Z get corrected at the order of 10^{-5}, which would also be the order of corrections to decay amplitudes. The partial decay widths of Z are known to about 3-digit accuracy [55], such that the bounds from neutrino-electron scattering are slightly more stringent.

Similar constraints also exist for model A, which should be approximately of the same magnitude. However, as we will see, the constraints from charged lepton decay are much more stringent than those from elastic neutrino scattering in model A.

Charged lepton flavor violation. Charged lepton flavor violation (CLFV) could cause rare lepton decays such as $\mu \to e\gamma$, $\mu \to 3e$, $\tau \to \mu\gamma$, etc. Currently all lepton flavor violating decays have not been observed, which yields very strong constraints on models containing CLFV. In this paper, we only need to consider CLFV in model A because the other two models only have flavor violations limited to the neutrino sector. Here we would like to refer to ref. [21] which has studied these decay processes in model A. We present the results in ref. [21] with the experimental bounds updated.

The CLFV decay widths in model A are given by

$$\Gamma(\ell_\alpha \to \ell_\beta \gamma) = \frac{1}{16\pi^2} \frac{g^2 s_W^2}{12} \left| \frac{\sum_\delta y_{\alpha\delta} y^*_{\beta\delta}}{m_\phi^2 G_F} \right|^2 \Gamma(\ell_\alpha \to \nu_\alpha \ell_\beta \overline{\nu_\beta}), \quad (4.17)$$

$$\Gamma(\ell_\alpha \to \ell_\beta \ell_{\beta'} \overline{\ell_{\beta'}}) = \frac{c_W^2}{g^2} \left| 2 g^{(1)}_{\alpha\beta} Q_Z^{(e_L)} \right|^2 \Gamma(\ell_\alpha \to \nu_\alpha \ell_\beta \overline{\nu_\beta}), \quad (4.18)$$

where $\ell_\alpha \to \nu_\alpha \ell_\beta \overline{\nu_\beta}$ is a SM charged current process. For example, the following branching ratios have been precisely measured [56]:

$$\text{Br}(\mu \to \nu_\mu e \overline{\nu_e}) \approx 100\%, \qquad \text{Br}(\tau \to \nu_\tau e \overline{\nu_e}) = (17.82 \pm 0.04)\%,$$
$$\text{Br}(\tau \to \nu_\tau \mu \overline{\nu_\mu}) = (17.39 \pm 0.04)\%. \quad (4.19)$$

The branching ratios with CLFV are highly suppressed, the following limits at 90% CL exist [56]:

$$\text{Br}(\mu \to e\gamma) < 5.7 \times 10^{-13}, \quad \text{Br}(\tau \to e\gamma) < 3.3 \times 10^{-8}, \quad \text{Br}(\tau \to \mu\gamma) < 4.4 \times 10^{-8}, \quad (4.20)$$

$$\text{Br}(\mu \to 3e) < 1.0 \times 10^{-12}, \quad \text{Br}(\tau \to 3e) < 2.7 \times 10^{-8}, \quad \text{Br}(\tau \to 3\mu) < 2.1 \times 10^{-8}. \quad (4.21)$$

JHEP10(2018)096

From the above data, we can derive the corresponding constraints on $g^{(1)}_{\alpha\beta}$ according to eqs. (4.17), (4.18), and (3.14):

$$|g^{(1)}_{\mu e}| < 8.9 \times 10^{-8}\ (\mu \to e\gamma), \qquad |g^{(1)}_{\tau e}| < 5.0 \times 10^{-5}\ (\tau \to e\gamma),$$
$$|g^{(1)}_{\tau\mu}| < 6.0 \times 10^{-5}\ (\tau \to \mu\gamma), \tag{4.22}$$
$$|g^{(1)}_{\mu e}| < 1.3 \times 10^{-6},\ (\mu \to 3e), \qquad |g^{(1)}_{\tau e}| < 5.1 \times 10^{-4}\ (\tau \to 3e),$$
$$|g^{(1)}_{\tau\mu}| < 4.5 \times 10^{-4}\ (\tau \to 3\mu). \tag{4.23}$$

Note that those bounds have a weak dependence on m_ϕ^2 due to the log $\frac{m_Z^2}{m_\phi^2}$ term in eq. (3.14). For simplicity, we have set $m_\phi = 500$ GeV. As one can see, the constraints in eq. (4.23) are weaker than eq. (4.22). Taking the values in eq. (4.22), we get

$$|\epsilon^{\triangleright}_{\mu e}| < 1.0 \times 10^{-6}\, Q_Z^{(\psi)}, \quad |\epsilon^{\triangleright}_{\tau e}| < 5.5 \times 10^{-4}\, Q_Z^{(\psi)}, \quad |\epsilon^{\triangleright}_{\tau\mu}| < 6.5 \times 10^{-4}\, Q_Z^{(\psi)}, \tag{4.24}$$

where $Q_Z^{(\psi)} = s_W^2 - \frac{1}{4}$, $-\frac{1}{4}$, or $\frac{1}{4} - s_W^2$, for $\psi = e$, or n, or p respectively.

Similar to $\epsilon^{\triangleright}_{\mu e}$, the CLFV constraints on $\epsilon^{\square}_{\alpha\beta}$ from $\ell_\alpha \to \ell_\beta\gamma$ are also more stringent than those from $\ell_\alpha \to \ell_\beta \ell_{\beta'} \overline{\ell_{\beta'}}$. According to eq. (4.17) and eq. (3.17), the bounds in eq. (4.20) cannot be directly converted to the bounds on $\epsilon^{\square}_{\alpha\beta}$ without known bounds on $|y_{e\mu}|^2 + |y_{e\tau}|^2$. So for simplicity, we set $|y_{e\mu}|^2,\ |y_{e\tau}|^2 < 1$, and get

$$\epsilon^{\square}_{\mu e} < 7.8 \times 10^{-6}, \quad \epsilon^{\square}_{\tau e} < 4.4 \times 10^{-3}, \quad \epsilon^{\square}_{\tau\mu} < 5.2 \times 10^{-3}. \tag{4.25}$$

Combining all the constraints discussed above, the strongest constraints on the loop-induced NSI parameters come from CLFV for model A, and elastic neutrino scattering for modela B and C. The results are summarized in table 2.

5 Conclusion

In scalar extensions of the SM, complex NSI can be generated at the loop level, denoted here loop-induced NSI. There are two types of loop diagrams that are responsible for loop-induced NSI, triangle diagrams and box diagrams shown in figure 1. We computed the loop diagrams and derived general formulae for loop-induced NSI, given by eqs. (2.8) and (2.19).

To be more concrete, we applied our results to three specific and frequently discussed models, which contain charged or neutral scalar bosons. With the experimental constraints on these models taken into consideration, we estimated how large the loop-induced NSI can be, which is summarized in table 2. Testable NSI are possible.

Our calculations were performed in the limit of heavy scalars (heavier than the fermion masses in loops), though a similar analysis could also be performed for light particles. Loop-induced NSI are not neccesarily obtainable by scalar particles only, but also by vector bosons, leptoquarks etc. The relevant phenomenology will differ and deserves future study.

Acknowledgments

IB is supported by the IMPRS-PTFS and enrolled at Heidelberg University. WR is supported by the DFG with grant RO 2516/6-1 in the Heisenberg program.

JHEP10(2018)096

A The triangle diagrams

In this appendix, we compute the triangle diagrams in a general U(1) model. The result can be directly applied to more complicated models such as the SM extended by various scalar particles. Various useful identities and relations necessary for our calculations can be found in appendix C.

The U(1) model being considered here contains a massive scalar ϕ and three massless fermions ψ_1, ψ_2 and ψ_3. They are all charged under the U(1) gauge symmetry so the Lagrangian is

$$\mathcal{L} = \sum_{i=1}^{3} \overline{\psi}_i i\not{D}_\mu \psi_i + |D_\mu \phi|^2 - m_\phi^2 \phi\phi^* + \left(y_{21}\overline{\psi}_2 \phi \psi_1 + y_{23}\overline{\psi}_2 \phi \psi_3 + \text{h.c.}\right), \tag{A.1}$$

where

$$D_\mu = \partial_\mu - igQA_\mu, \quad Q = \begin{cases} Q_\phi & \text{for } \phi \\ Q_i & \text{for } \psi_i \end{cases}. \tag{A.2}$$

In eq. (A.1) we have included only two Yukawa couplings y_{12} and y_{23} because this is the minimal requirement to obtain the effective flavor-changing operator $A_\mu \overline{\psi}_1 \gamma^\mu \psi_3$ at the 1-loop level, as indicated in figure 3. Including other Yukawa terms ($\overline{\psi}_1 \phi \psi_3$ or $\overline{\psi}_1 \phi^* \psi_3$) would only complicate the scenario and may not allowed by the U(1) charges.[10] Due to the U(1) charge conservation, the Yukawa interactions in eq. (A.1) are allowed when

$$Q_\phi - Q_2 + Q_1 = Q_\phi - Q_2 + Q_3 = 0, \tag{A.3}$$

which further implies

$$Q_1 = Q_3.$$

There are two potential problems when applying the above U(1) model to SM extensions. First, the Z boson in the SM is massive while here the U(1) gauge boson is massless if the gauge symmetry is unbroken. To make the result in this appendix applicable to massive gauge bosons, we manually introduce a mass m_A for the gauge boson. The gauge boson mass could be generated by introduce another scalar field with spontaneous symmetry breaking but we would rather refrain from involving such details.

Another problem is about the chiral fermions. The SM, as a chiral theory of fermions, has different gauge interactions for left–handed and right-handed fermions. For example, e_L and e_R have different Z-vertices. The U(1) model considered here is parity conserving, i.e. both the left-handed and right-handed components of ψ_i are equally coupled to the gauge and scalar bosons. This problem can be easily solved if the Dirac spinors are decomposed into Weyl spinors. In the U(1) model, the two sets of Weyl components (ψ_{L1}, ψ_{R2}, ψ_{L3}) and (ψ_{R1}, ψ_{L2}, ψ_{R3}) do not couple to each other directly because

$$\overline{\psi}_i i\not{D}_\mu \psi_i = \overline{\psi}_{Li} i\not{D}_\mu \psi_{Li} + \overline{\psi}_{Ri} i\not{D}_\mu \psi_{Ri}, \tag{A.4}$$

$$\overline{\psi}_2 \phi \psi_1 = \overline{\psi}_{R2} \phi \psi_{L1} + \overline{\psi}_{L2} \phi \psi_{R1}, \tag{A.5}$$

$$\overline{\psi}_2 \phi \psi_3 = \overline{\psi}_{R2} \phi \psi_{L3} + \overline{\psi}_{L2} \phi \psi_{R3}. \tag{A.6}$$

[10] For example, if $|Q_\phi| \neq Q_1 - Q_3$, the 1-3 Yukawa mixing terms can be forbidden by the U(1) symmetry.

JHEP10(2018)096

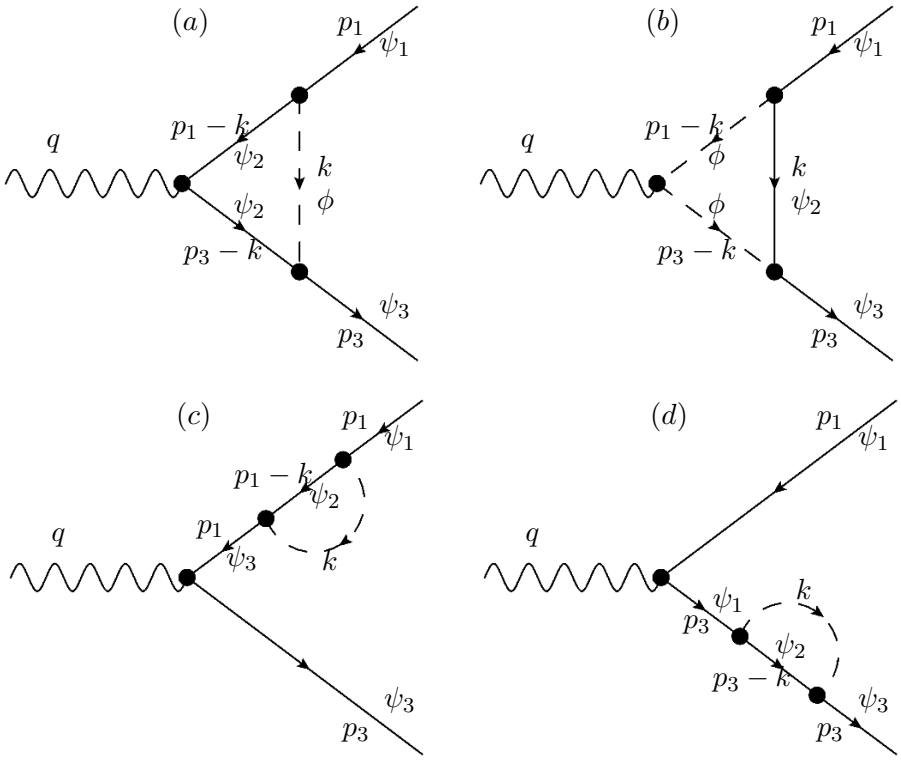

Figure 3. Triangle diagrams that give rise to the effective flavor-changing operator. The UV divergences of these diagrams should cancel in the summation due to gauge invariance.

Therefore, in the diagrams in figure 3, all the fermion lines can also be regarded as either $(\psi_{L1},\ \psi_{R2},\ \psi_{L3})$ or $(\psi_{R1},\ \psi_{L2},\ \psi_{R3})$. At the end of this section, we will also present the result for a chiral U(1).

It is important to notice that the sum of all the four diagrams in figure 3 is finite, as pointed out in ref. [20]. The UV divergences necessarily cancel out if the model is renormalizable, otherwise there is no corresponding counter term to cancel the infinity. We will show the cancellation explicitly in the following calculation.

Now let us compute the four diagrams (a)–(d) in figure 3. The relevant interactions are

$$\mathcal{L} \supset y_{21}\overline{\psi}_2\phi\psi_1 + y_{23}^*\overline{\psi}_3\phi^*\psi_2 + g\sum_i Q_i A_\mu \overline{\psi}_i\gamma^\mu\psi_i + igQ_\phi A^\mu\phi^* \overleftrightarrow{\partial}_\mu \phi, \tag{A.7}$$

where $\phi^* \overleftrightarrow{\partial}_\mu \phi \equiv \phi^*\partial_\mu\phi - \phi\partial_\mu\phi^*$. Then it is straightforward to write down the amplitudes

$$i\mathcal{M}_a = \int \frac{d^4k}{(2\pi)^4}\overline{u}(p_3)iy_{23}^*\frac{i}{(p_3-k)\cdot\gamma}igQ_2\gamma^\mu\epsilon_\mu(q)\frac{i}{(p_1-k)\cdot\gamma}iy_{21}\frac{i}{k^2-m_\phi^2}u(p_1), \tag{A.8}$$

$$i\mathcal{M}_b = \int \frac{d^4k}{(2\pi)^4}\overline{u}(p_3)iy_{23}^*\frac{i}{\not{k}}iy_{21}\frac{i}{(p_3-k)^2-m_\phi^2} \times \left[-igQ_\phi(p_1+p_3-2k)^\mu\right]\epsilon_\mu(q)\frac{i}{(p_1-k)^2-m_\phi^2}u(p_1), \tag{A.9}$$

JHEP10(2018)096

$$i\mathcal{M}_c = \int \frac{d^4k}{(2\pi)^4} \overline{u}(p_3) i g Q_3 \gamma^\mu \epsilon_\mu(q) \frac{i}{\not{p}_1 - m_3} i y_{23}^* \frac{i}{(p_1 - k)\cdot\gamma} i y_{21} \frac{i}{k^2 - m_\phi^2} u(p_1), \tag{A.10}$$

$$i\mathcal{M}_d = \int \frac{d^4k}{(2\pi)^4} \overline{u}(p_3) i y_{23}^* \frac{i}{(p_3 - k)\cdot\gamma} \frac{i}{k^2 - m_\phi^2} i y_{21} \frac{i}{\not{p}_3 - m_1} i g Q_1 \gamma^\mu \epsilon_\mu(q) u(p_1). \tag{A.11}$$

Here we assume that the fermions $\psi_{1,3}$ have very small masses $m_{1,3}$ so that the standard technique of extracting form factors can be applied. After that, we will take the limit $m_{1,3} \to 0$. For simplicity, we evaluate the amplitudes with all external momenta on shell so that amplitudes can be organized by three form factors F_1, F_2 and F_3 as follows

$$\begin{aligned} &i\mathcal{M}_a + i\mathcal{M}_b + i\mathcal{M}_c + i\mathcal{M}_d \\ &\quad = \overline{u}(p_3) \left[\left(\gamma^\mu - \frac{\not{q} q^\mu}{q^2} \right) F_1(q^2) + \frac{i\sigma^{\mu\nu} q_\nu}{m_1 + m_3} F_2(q^2) + \frac{2q^\mu}{m_1 + m_3} F_3(q^2) \right] u(p_1) \epsilon_\mu(q). \end{aligned} \tag{A.12}$$

Since $\not{q} = \not{p}_3 - \not{p}_1$ and $\not{p}_1 u(p_1) = m_1$, $\overline{u}(p_3)\not{p}_3 = m_3$, the F_1 term actually reduces to $\gamma^\mu F_1(q^2)$ in the zero mass limit ($m_{1,3} \to 0$). We use the computer program `Package-X` [57] to compute the loop integrals in dimensional regularization. The form factors can be directly extracted by using the corresponding projectors in `Package-X`. In this paper, we are only interested in the F_1 form factor. Let us first check the UV divergence in F_1. Since we are using dimensional regularization, the UV divergent part is proportional to $1/\epsilon \equiv 2/(d-4)$:

$$F_1^{(\text{divergent})} = \frac{g y_{23}^* y_{21}}{2\epsilon} \left(Q_2 - Q_\phi + \frac{-Q_3 m_1}{m_1 - m_3} + \frac{Q_1 m_3}{m_1 - m_3} \right), \tag{A.13}$$

where the terms proportional to Q_2, Q_ϕ, Q_3, and Q_1 correspond to the contributions of diagrams (a), (b), (c), and (d), respectively (note that each of these diagrams has a distinct gauge interaction vertex and a characteristic U(1) charge). Eq. (A.13) can also be written as

$$F_1^{(\text{divergent})} = \frac{g y_{23}^* y_{21}}{2\epsilon} \frac{m_3(Q_\phi - Q_2 + Q_1) - m_1(Q_\phi - Q_2 + Q_3)}{m_1 - m_3}, \tag{A.14}$$

which, according to eq. (A.3), implies that the UV divergence vanishes if the U(1) charges are conserved.

Taking $Q_3 = Q_1$, $Q_\phi = Q_2 - Q_1$ and $(m_1,\ m_3) \to 0$, the finite part of F_1 is

$$F_1^{(\text{finite})} = \frac{i g y_{23}^* y_{21} \left(f(r) Q_1 + h(r) Q_2 \right)}{16\pi^2}, \tag{A.15}$$

with

$$r \equiv \frac{m_A^2}{m_\phi^2}, \tag{A.16}$$

$$\omega \equiv -r - i0^+, \tag{A.17}$$

$$f(r) = \frac{1}{4\omega} \left[-4C_{101}(\omega) + 2(\omega+2) B_{0\Lambda}(\omega) + 5\omega + 4 \right], \tag{A.18}$$

$$h(r) = \frac{1}{4\omega} \left[4C_{010}(\omega) + 4C_{101}(\omega) + 2(\omega+2) \left(\log \frac{1}{\omega} - B_{0\Lambda}(\omega) \right) - 4\omega \right]. \tag{A.19}$$

JHEP10(2018)096

Here $B_{0\Lambda}$, C_{101}, C_{010} are parts of the scalar Passarino-Veltman functions, with the explicit forms given below:

$$B_{0\Lambda}(\omega) = -\frac{1}{\omega}\sqrt{\omega(\omega+4)}\log\left(\frac{\omega+\sqrt{\omega(\omega+4)}+2}{2}\right), \tag{A.20}$$

$$\begin{aligned} C_{101}(\omega) = {} & \frac{\pi^2}{6\omega} + \frac{1}{2\omega}\left[\log^2\left(\frac{\omega-\sqrt{\omega(\omega+4)}}{2\omega}\right) - \log^2\left(\frac{\omega+\sqrt{\omega(\omega+4)}+2}{\sqrt{\omega(\omega+4)}-\omega}\right)\right] \\ & - \frac{1}{\omega}\mathrm{Li}_2(\omega+1) - \frac{1}{\omega}\mathrm{Li}_2\left(\frac{2(\omega+1)}{\omega-\sqrt{\omega(\omega+4)}}\right) + \frac{1}{\omega}\mathrm{Li}_2\left(\frac{2}{\sqrt{\omega(\omega+4)}-\omega}\right) \\ & - \frac{1}{\omega}\mathrm{Li}_2\left(\frac{2}{\omega+\sqrt{\omega(\omega+4)}+2}\right) + \frac{1}{\omega}\mathrm{Li}_2\left(\frac{1}{2}(\omega+1)\left(\omega+\sqrt{\omega(\omega+4)}+2\right)\right), \end{aligned} \tag{A.21}$$

$$C_{010}(\omega) = -\frac{6\mathrm{Li}_2\left(\frac{\omega-1}{\omega}\right) + 3\log^2\left(\frac{1}{\omega}\right) + \pi^2}{6\omega}. \tag{A.22}$$

Using the identities of the dilogarithm function (C.12)–(C.14), we can make a series expansion in r and obtain eq. (2.13) and eq. (2.14).

In summary, the triangle diagrams can generate the following effective vector vertex

$$\mathcal{L}_{\text{eff}} = g_{31}^{(1)} A_\mu \overline{\psi}_3 \gamma^\mu \psi_1, \tag{A.23}$$

where

$$g_{31}^{(1)} = \frac{g y_{23}^* y_{21}}{16\pi^2}\left(f(r)Q_1 + h(r)Q_2\right). \tag{A.24}$$

Note that the result is applicable only when the U(1) charges are conserved—see eq. (A.3).

For a chiral U(1) theory, we can still use the above result by simply replacing the Dirac spinors with the chiral spinors. For example, if only $(\psi_{L1},\ \psi_{R2},\ \psi_{L3})$ are present in the model, then we have

$$\mathcal{L}_{\text{eff}} = g_{31}^{(1)} A_\mu \overline{\psi}_{L3} \gamma^\mu \psi_{L1} = g_{31}^{(1)} A_\mu \overline{\psi}_3 \gamma^\mu P_L \psi_1, \tag{A.25}$$

where $g_{31}^{(1)}$ is the same as eq. (A.24), and $(Q_1,\ Q_2,\ Q_3)$ should be the U(1) charges of $(\psi_{L1},\ \psi_{R2},\ \psi_{L3})$ respectively.

B The box diagram

This appendix computes the box diagram in a general model with six fermions ψ_i $(i = 1, 2, \cdots, 6)$ and one complex scalar field ϕ, with the following Yukawa interactions:

$$\begin{aligned} \mathcal{L} \supset {} & y_{21}\overline{\psi}_2\phi\psi_1 + y_{23}\overline{\psi}_2\phi\psi_3 + y_{45}\overline{\psi}_4\phi\psi_5 + y_{65}\overline{\psi}_6\phi\psi_5 \\ & + y_{21}^*\overline{\psi}_1\phi^*\psi_2 + y_{23}^*\overline{\psi}_3\phi^*\psi_2 + y_{45}^*\overline{\psi}_5\phi^*\psi_4 + y_{65}^*\overline{\psi}_5\phi^*\psi_6. \end{aligned} \tag{B.1}$$

The second line is just the hermitian conjugate of the first line. For convenience of later use, we write the hermitian conjugate terms explicitly.

JHEP10(2018)096

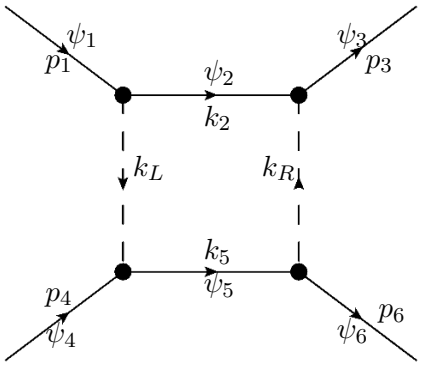

Figure 4. Box diagram that generates the effective four-fermion operator $\overline{\psi}_3\gamma^\mu\psi_1\overline{\psi}_6\gamma_\mu\psi_4$.

The box diagram we will compute is shown in figure 4, according to which we can straightforwardly write down the amplitude

$$i\mathcal{M}_{\text{box}} = \int \frac{d^4k}{(2\pi)^4}\overline{u}(p_3)iy_{23}^*\frac{i}{\not{k}_2}iy_{21}u(p_1)\frac{i}{k_L^2-m_\phi^2}\frac{i}{k_R^2-m_\phi^2}\overline{u}(p_6)iy_{65}\frac{i}{\not{k}_5}iy_{45}^*u(p_4). \tag{B.2}$$

where the fermions are all massless and the scalar has mass m_ϕ^2.

The amplitude is finite and can be computed directly. Since we are interested in the heavy scalar mass limit, let us take the zero external momentum limit $(p_1,\ p_3,\ p_4,\ p_6)/m_\phi \to 0$:

$$i\mathcal{M}_{\text{box}} = \overline{u}(p_3)iy_{23}^*\gamma^\mu iy_{21}u(p_1)\overline{u}(p_6)iy_{65}\gamma^\nu iy_{45}^*u(p_4)I(m_\phi^2,\ m_\phi^2), \tag{B.3}$$

where we define the integral

$$I(m_a^2,\ m_b^2) = \int \frac{d^4k}{(2\pi)^4}\frac{i(-k^\mu)}{k^2}\frac{i(k^\nu)}{k^2}\frac{i}{k^2-m_a^2}\frac{i}{k^2-m_b^2}. \tag{B.4}$$

It can be evaluated straightforwardly:

$$I(m_a^2,\ m_b^2) = \frac{i}{16\pi^2}\frac{\log\left(\frac{m_a^2}{m_b^2}\right)g^{\mu\nu}}{4\left(m_a^2-m_b^2\right)}. \tag{B.5}$$

In the equal mass limit $(m_a^2 = m_b^2 = m_\phi^2)$, it is

$$I(m_\phi^2,\ m_\phi^2) = \frac{i}{16\pi^2}\frac{1}{4m_\phi^2}g^{\mu\nu}. \tag{B.6}$$

In summary, the box diagram generates the following four-fermion effect operator

$$\mathcal{L}_{\text{eff}} = \frac{1}{16\pi^2}\frac{y_{23}^*y_{21}y_{65}y_{45}^*}{4m_\phi^2}\overline{\psi}_3\gamma^\mu\psi_1\overline{\psi}_6\gamma_\mu\psi_4 \tag{B.7}$$

$$= \frac{1}{16\pi^2}\frac{y_{23}^*y_{21}y_{65}y_{45}^*}{4m_\phi^2}\overline{\psi}_3\gamma^\mu\psi_1\overline{\psi_4^c}(-\gamma_\mu)\psi_6^c. \tag{B.8}$$

JHEP10(2018)096

C Some useful identities and transformations

In this work, we need to frequently transform Dirac matrices and spinor products from one to another. Besides, in the loop calculation, we also need some useful identities about the dilogarithm functions. Therefore, we compile them in this appendix.

The left- and right-handed projectors are defined as

$$P_L \equiv \frac{1-\gamma^5}{2},\ P_R \equiv \frac{1+\gamma^5}{2}. \tag{C.1}$$

Products of $P_{L/R}$ with the Dirac matrices can be transformed using

$$\gamma^5 P_L = P_L \gamma^5 = -P_L, \qquad P_R\gamma^5 = \gamma^5 P_R = P_R, \tag{C.2}$$

$$\gamma_\mu\gamma^5 = -\gamma^5\gamma_\mu, \qquad \gamma^\mu P_L = P_R\gamma^\mu, \qquad \gamma^\mu P_R = P_L\gamma^\mu. \tag{C.3}$$

Defining

$$\sigma_{\mu\nu} \equiv \frac{i}{2}[\gamma^\mu,\ \gamma^\nu], \tag{C.4}$$

we also have

$$P_L\sigma_{\mu\nu} = \sigma_{\mu\nu}P_L,\ P_R\sigma_{\mu\nu} = \sigma_{\mu\nu}P_R.$$

The left- and right-handed components of a Dirac spinor ψ are defined as

$$\psi_L \equiv P_L\psi,\quad \psi_R \equiv P_R\psi. \tag{C.5}$$

The charge conjugate of ψ is defined as

$$\psi^c \equiv -i\gamma^2\psi^*. \tag{C.6}$$

The left- and right-handed projections and the charge conjugation are related by

$$\overline{\psi_L} = \overline{\psi}P_R, \qquad \overline{\psi_R} = \overline{\psi}P_L, \tag{C.7}$$

$$\psi^c_L \equiv (\psi_L)^c = -i\gamma^2 P_L\psi^* = P_R\psi^c. \tag{C.8}$$

For two different Dirac spinors ψ_1 and ψ_2, we have

$$\overline{\psi^c_1}\psi_2 = \overline{\psi^c_2}\psi_1, \qquad \overline{\psi_1}\psi^c_2 = \overline{\psi_2}\psi^c_1, \qquad \overline{\psi^c_1}\psi^c_2 = \overline{\psi_2}\psi_1, \tag{C.9}$$

$$\overline{\psi^c_1}\gamma^\mu\psi^c_2 = -\overline{\psi_2}\gamma^\mu\psi_1. \tag{C.10}$$

Turning to loop-functions needed in this study, the dilogarithm $\mathrm{Li}_2(z)$ can be defined by

$$\mathrm{Li}_2(z) = \sum_{k=1}^{\infty}\frac{z^k}{k^2} = \int_z^0 \frac{\log(1-t)}{t}dt. \tag{C.11}$$

It has a branch cut at $z > 1$, so in many cases we need the following identities

$$\mathrm{Li}_2\left(\frac{1}{z}\right) = -\mathrm{Li}_2(z) - \frac{1}{2}\log^2(-z) - \frac{\pi^2}{6}, \tag{C.12}$$

$$\mathrm{Li}_2\left(1-\frac{1}{z}\right) = \mathrm{Li}_2(z) - \frac{1}{2}\log^2(z) + \log(1-z)\log(z) - \frac{\pi^2}{6}, \tag{C.13}$$

$$\mathrm{Li}_2(1-z) = -\mathrm{Li}_2(z) - \log(1-z)\log(z) + \frac{\pi^2}{6}, \tag{C.14}$$

to transform some dilogarithmic singularities to logarithmic singularities which are easier to handle.

JHEP10(2018)096

References

[1] F. Capozzi et al., *Neutrino masses and mixings: status of known and unknown* 3ν *parameters*, *Nucl. Phys.* **B 908** (2016) 218 [arXiv:1601.07777] [INSPIRE].

[2] I. Esteban et al., *Updated fit to three neutrino mixing: exploring the accelerator-reactor complementarity*, *JHEP* **01** (2017) 087 [arXiv:1611.01514] [INSPIRE].

[3] P.F. de Salas et al., *Status of neutrino oscillations 2018:* 3σ *hint for normal mass ordering and improved CP sensitivity*, *Phys. Lett.* **B 782** (2018) 633 [arXiv:1708.01186] [INSPIRE].

[4] S. Davidson, C. Pena-Garay, N. Rius and A. Santamaria, *Present and future bounds on nonstandard neutrino interactions*, *JHEP* **03** (2003) 011 [hep-ph/0302093] [INSPIRE].

[5] T. Ohlsson, *Status of non-standard neutrino interactions*, *Rept. Prog. Phys.* **76** (2013) 044201 [arXiv:1209.2710] [INSPIRE].

[6] Y. Farzan and M. Tortola, *Neutrino oscillations and non-standard interactions*, *Front. Phys.* **6** (2018) 10 [arXiv:1710.09360].

[7] I. Esteban et al., *Updated constraints on non-standard interactions from global analysis of oscillation data*, *JHEP* **08** (2018) 180 [arXiv:1805.04530] [INSPIRE].

[8] M. Masud, A. Chatterjee and P. Mehta, *Probing CP-violation signal at DUNE in presence of non-standard neutrino interactions*, *J. Phys.* **G 43** (2016) 095005 [arXiv:1510.08261] [INSPIRE].

[9] A. de Gouvêa and K.J. Kelly, *Non-standard neutrino interactions at DUNE*, *Nucl. Phys.* **B 908** (2016) 318 [arXiv:1511.05562] [INSPIRE].

[10] M. Masud and P. Mehta, *Nonstandard interactions spoiling the CP-violation sensitivity at DUNE and other long baseline experiments*, *Phys. Rev.* **D 94** (2016) 013014 [arXiv:1603.01380] [INSPIRE].

[11] M. Masud and P. Mehta, *Nonstandard interactions and resolving the ordering of neutrino masses at DUNE and other long baseline experiments*, *Phys. Rev.* **D 94** (2016) 053007 [arXiv:1606.05662] [INSPIRE].

[12] M. Blennow et al., *A combined study of source, detector and matter non-standard neutrino interactions at DUNE*, *JHEP* **08** (2016) 090 [arXiv:1606.08851] [INSPIRE].

[13] S.K. Agarwalla, S.S. Chatterjee and A. Palazzo, *Degeneracy between* θ_{23} *octant and neutrino non-standard interactions at DUNE*, *Phys. Lett.* **B 762** (2016) 64 [arXiv:1607.01745] [INSPIRE].

[14] K.N. Deepthi, S. Goswami and N. Nath, *Challenges posed by non-standard neutrino interactions in the determination of* δ_{CP} *at DUNE*, *Nucl. Phys.* **B 936** (2018) 91 [arXiv:1711.04840] [INSPIRE].

[15] W. Konetschny and W. Kummer, *Nonconservation of total lepton number with scalar bosons*, *Phys. Lett.* **70B** (1977) 433 [INSPIRE].

[16] T.P. Cheng and L.-F. Li, *Neutrino masses, mixings and oscillations in* $\mathrm{SU}(2) \times \mathrm{U}(1)$ *models of electroweak interactions*, *Phys. Rev.* **D 22** (1980) 2860 [INSPIRE].

JHEP10(2018)096

[17] J. Schechter and J.W.F. Valle, *Neutrino masses in* SU(2) × U(1) *theories*, *Phys. Rev.* **D 22** (1980) 2227 [INSPIRE].

[18] X.-J. Xu, *Minima of the scalar potential in the type-II seesaw model: from local to global*, *Phys. Rev.* **D 94** (2016) 115025 [arXiv:1612.04950] [INSPIRE].

[19] M. Malinsky, T. Ohlsson and H. Zhang, *Non-standard neutrino interactions from a triplet seesaw model*, *Phys. Rev.* **D 79** (2009) 011301 [arXiv:0811.3346] [INSPIRE].

[20] M.S. Bilenky and A. Santamaria, *One loop effective Lagrangian for a standard model with a heavy charged scalar singlet*, *Nucl. Phys.* **B 420** (1994) 47 [hep-ph/9310302] [INSPIRE].

[21] S. Antusch, J.P. Baumann and E. Fernandez-Martinez, *Non-standard neutrino interactions with matter from physics beyond the standard model*, *Nucl. Phys.* **B 810** (2009) 369 [arXiv:0807.1003] [INSPIRE].

[22] M.B. Wise and Y. Zhang, *Effective theory and simple completions for neutrino interactions*, *Phys. Rev.* **D 90** (2014) 053005 [arXiv:1404.4663] [INSPIRE].

[23] D.V. Forero and W.-C. Huang, *Sizable NSI from the* $SU(2)_L$ *scalar doublet-singlet mixing and the implications in DUNE*, *JHEP* **03** (2017) 018 [arXiv:1608.04719] [INSPIRE].

[24] J. Herrero-García, T. Ohlsson, S. Riad and J. Wirén, *Full parameter scan of the Zee model: exploring Higgs lepton flavor violation*, *JHEP* **04** (2017) 130 [arXiv:1701.05345] [INSPIRE].

[25] U.K. Dey, N. Nath and S. Sadhukhan, *Non-standard neutrino interactions in a modified ν2HDM*, *Phys. Rev.* **D 98** (2018) 055004 [arXiv:1804.05808] [INSPIRE].

[26] J. Heeck and W. Rodejohann, *Gauged* L_μ–L_τ *symmetry at the electroweak scale*, *Phys. Rev.* **D 84** (2011) 075007 [arXiv:1107.5238] [INSPIRE].

[27] T. Ohlsson, T. Schwetz and H. Zhang, *Non-standard neutrino interactions in the Zee-Babu model*, *Phys. Lett.* **B 681** (2009) 269 [arXiv:0909.0455] [INSPIRE].

[28] C. Giunti and C.W. Kim, *Fundamentals of neutrino physics and astrophysics*, Oxford University Press, Oxford U.K. (2007).

[29] S. Bergmann, Y. Grossman and E. Nardi, *Neutrino propagation in matter with general interactions*, *Phys. Rev.* **D 60** (1999) 093008 [hep-ph/9903517] [INSPIRE].

[30] Y. Farzan, *A model for large non-standard interactions of neutrinos leading to the LMA-Dark solution*, *Phys. Lett.* **B 748** (2015) 311 [arXiv:1505.06906] [INSPIRE].

[31] Y. Farzan and J. Heeck, *Neutrinophilic nonstandard interactions*, *Phys. Rev.* **D 94** (2016) 053010 [arXiv:1607.07616] [INSPIRE].

[32] A. Zee, *A theory of lepton number violation, neutrino Majorana mass, and oscillation*, *Phys. Lett.* **B 93** (1980) 389 [*Erratum ibid.* **B 95** (1980) 961].

[33] E.W. Kolb and M.S. Turner, *Supernova SN 1987a and the secret interactions of neutrinos*, *Phys. Rev.* **D 36** (1987) 2895 [INSPIRE].

[34] M.S. Bilenky, S.M. Bilenky and A. Santamaria, *Invisible width of the Z boson and 'secret' neutrino-neutrino interactions*, *Phys. Lett.* **B 301** (1993) 287 [INSPIRE].

[35] S. Hannestad, R.S. Hansen and T. Tram, *How self-interactions can reconcile sterile neutrinos with cosmology*, *Phys. Rev. Lett.* **112** (2014) 031802 [arXiv:1310.5926] [INSPIRE].

[36] K.C.Y. Ng and J.F. Beacom, *Cosmic neutrino cascades from secret neutrino interactions*, *Phys. Rev.* **D 90** (2014) 065035 [*Erratum ibid.* **D 90** (2014) 089904] [arXiv:1404.2288] [INSPIRE].

JHEP10(2018)096

[37] F. Forastieri, M. Lattanzi and P. Natoli, *Constraints on secret neutrino interactions after Planck*, *JCAP* **07** (2015) 014 [arXiv:1504.04999] [INSPIRE].

[38] G.-Y. Huang, T. Ohlsson and S. Zhou, *Observational constraints on secret neutrino interactions from Big Bang nucleosynthesis*, *Phys. Rev.* **D 97** (2018) 075009 [arXiv:1712.04792] [INSPIRE].

[39] J. Chakrabortty, P. Ghosh and W. Rodejohann, *Lower limits on $\mu \to e\gamma$ from New Measurements on U_{e3}*, *Phys. Rev.* **D 86** (2012) 075020 [arXiv:1204.1000] [INSPIRE].

[40] Y. Chikashige, R.N. Mohapatra and R.D. Peccei, *Are there real Goldstone bosons associated with broken lepton number?*, *Phys. Lett.* **B 98** (1981) 265.

[41] J.W.F. Valle, *Gauge theories and the physics of neutrino mass*, *Prog. Part. Nucl. Phys.* **26** (1991) 91 [INSPIRE].

[42] COHERENT collaboration, D. Akimov et al., *Observation of coherent elastic neutrino-nucleus scattering*, *Science* **357** (2017) 1123 [arXiv:1708.01294] [INSPIRE].

[43] C. Buck et al., *The CONUS experiment*, talk given at *Topics in Astroparticle and Underground Physics (TAUP 2017)*, July 24–28, Laurentian University, Sudbury, Canada (2017).

[44] CHARM-II collaboration, P. Vilain et al., *Measurement of differential cross-sections for muon-neutrino electron scattering*, *Phys. Lett.* **B 302** (1993) 351 [INSPIRE].

[45] CHARM-II collaboration, P. Vilain et al., *Precision measurement of electroweak parameters from the scattering of muon-neutrinos on electrons*, *Phys. Lett.* **B 335** (1994) 246 [INSPIRE].

[46] LSND collaboration, L.B. Auerbach et al., *Measurement of electron-neutrino-electron elastic scattering*, *Phys. Rev.* **D 63** (2001) 112001 [hep-ex/0101039] [INSPIRE].

[47] TEXONO collaboration, M. Deniz et al., *Measurement of neutrino-electron scattering cross-section with a CsI(Tl) scintillating crystal array at the Kuo-Sheng nuclear power reactor*, *Phys. Rev.* **D 81** (2010) 072001 [arXiv:0911.1597] [INSPIRE].

[48] A.G. Beda et al., *GEMMA experiment: three years of the search for the neutrino magnetic moment*, *Phys. Part. Nucl. Lett.* **7** (2010) 406 [arXiv:0906.1926] [INSPIRE].

[49] A.G. Beda et al., *Upper limit on the neutrino magnetic moment from three years of data from the GEMMA spectrometer*, arXiv:1005.2736 [INSPIRE].

[50] M. Lindner, W. Rodejohann and X.-J. Xu, *Coherent neutrino-nucleus scattering and new neutrino interactions*, *JHEP* **03** (2017) 097 [arXiv:1612.04150] [INSPIRE].

[51] M. Lindner, F.S. Queiroz, W. Rodejohann and X.-J. Xu, *Neutrino-electron scattering: general constraints on Z' and dark photon models*, *JHEP* **05** (2018) 098 [arXiv:1803.00060] [INSPIRE].

[52] Y. Farzan, M. Lindner, W. Rodejohann and X.-J. Xu, *Probing neutrino coupling to a light scalar with coherent neutrino scattering*, *JHEP* **05** (2018) 066 [arXiv:1802.05171] [INSPIRE].

[53] SLD Electroweak Group, DELPHI, ALEPH, SLD, SLD Heavy Flavour Group, OPAL, LEP Electroweak Working Group, L3 collaboration, S. Schael et al., *Precision electroweak measurements on the Z resonance*, *Phys. Rept.* **427** (2006) 257 [hep-ex/0509008] [INSPIRE].

[54] B. Sevda et al., *Constraints on nonstandard intermediate boson exchange models from neutrino-electron scattering*, *Phys. Rev.* **D 96** (2017) 035017 [arXiv:1702.02353] [INSPIRE].

JHEP10(2018)096

[55] Particle Data Group collaboration, M. Tanabashi et al., *Review of particle physics*, *Phys. Rev.* **D 98** (2018) 030001 [INSPIRE].

[56] Particle Data Group collaboration, C. Patrignani et al., *Review of particle physics*, *Chin. Phys.* **C 40** (2016) 100001 [INSPIRE].

[57] H.H. Patel, *Package-X: a Mathematica package for the analytic calculation of one-loop integrals*, *Comput. Phys. Commun.* **197** (2015) 276 [arXiv:1503.01469] [INSPIRE].

JHEP10(2018)096